Published online 14 May 2018

Nucleic Acids Research, 2018, Vol. 46, No. 11 ***5355–5365***
doi: 10.1093/nar/gky385

Cell penetrating thiazole peptides inhibit *c-MYC* expression via site-specific targeting of *c-MYC* G-quadruplex

Debasish Dutta[1,†], Manish Debnath[1,†], Diana Müller[2], Rakesh Paul[1], Tania Das[1], Irene Bessi[2], Harald Schwalbe[2] and Jyotirmayee Dash[1,*]

[1]Department of Organic Chemistry, Indian Association for the Cultivation of Science, Kolkata 700032, India and [2]Institute of Organic Chemistry and Chemical Biology, Center for Biomolecular Magnetic Resonance (BMRZ), Goethe University Frankfurt, Max-von-Laue Strasse 7, 60438 Frankfurt am Main, Germany

Received January 06, 2018; Revised April 06, 2018; Editorial Decision April 25, 2018; Accepted May 02, 2018

ABSTRACT

The structural differences among different G-quadruplexes provide an opportunity for site-specific targeting of a particular G-quadruplex structure. However, majority of G-quadruplex ligands described thus far show little selectivity among different G-quadruplexes. In this work, we delineate the design and synthesis of a crescent-shaped thiazole peptide that preferentially stabilizes *c-MYC* quadruplex over other promoter G-quadruplexes and inhibits *c-MYC* oncogene expression. Biophysical analysis such as Förster resonance energy transfer (FRET) melting and fluorescence spectroscopy show that the thiazole peptide TH3 can selectively interact with the *c-MYC* G-quadruplex over other investigated G-quadruplexes and duplex DNA. NMR spectroscopy reveals that peptide TH3 binds to the terminal G-quartets and capping regions present in the 5′- and 3′-ends of *c-MYC* G-quadruplex with a 2:1 stoichiometry; whereas structurally related distamycin A is reported to interact with quadruplex structures via groove binding and end stacking modes with 4:1 stoichiometry. Importantly, qRT-PCR, western blot and dual luciferase reporter assay show that TH3 down-regulates *c-MYC* expression by stabilizing the *c-MYC* G-quadruplex in cancer cells. Moreover, TH3 localizes within the nucleus of cancer cells and exhibits antiproliferative activities by inducing S phase cell cycle arrest and apoptosis.

INTRODUCTION

G-quadruplexes are four stranded DNA secondary structures that are hypothesized to be involved in key biological processes such as telomere maintenance and oncogene expression (1–3). G-quadruplex forming sequences are abundant in the promoter region of various proto-oncogenes like *c-MYC* (4), *c-KIT* (5), *BCL-2* (6) etc. The 27-mer G-quadruplex forming sequence located in the nuclease hypersensitive element (NHE) III1 of the *c-MYC* promoter region is well studied (7). It has been reported that this sequence exists in equilibrium between transcriptionally active forms (double helical and single stranded) and a silenced form (G-quadruplex) and regulates up to 90% of *c-MYC* transcription (8). This 27-mer sequence contains five consecutive runs of guanines, with three runs composed of four guanines each and two runs composed of three guanines each (*c-MYC*Pu27). However, only four runs of guanines are required to form G-quadruplex structure. It was reported that the predominant and biologically relevant G-quadruplex conformer of the *c-MYC* silencer element is a parallel-stranded G-quadruplex with 1:2:1 side loops (formed using the second, third, fourth, and fifth G-runs) (9–10). Small molecules that stabilize the specific *c-MYC* G-quadruplex structure can regulate expression of *c-MYC* oncogene at the transcriptional level (11–18). However, all G-quadruplexes contain G-quartets as a common structural feature, making it challenging to develop ligands selective for a particular G-quadruplex.

Most G-quadruplex ligands bind to the terminal G-quartet of G-quadruplex structures via end stacking mode. The groove (19–23) and intermediate regions of G-quadruplexes are different from each other, which may provide an opportunity to target a particular G-quadruplex structure. So far, very few ligands are reported to show selectivity among different G-quadruplex structures. In this work, we report the design and synthesis of novel thiazole peptides and the study of their interaction with four promoter G-quadruplexes (*c-MYC, c-KIT1, c-KIT2, BCL-2*) and a control duplex DNA. The interaction of these thia-

*To whom correspondence should be addressed. Tel: +91 33 2473 4971 (Ext. 1405); Email: ocjd@iacs.res.in
†The authors wish it to be known that, in their opinion, the first two authors should be regarded as Joint First Authors.

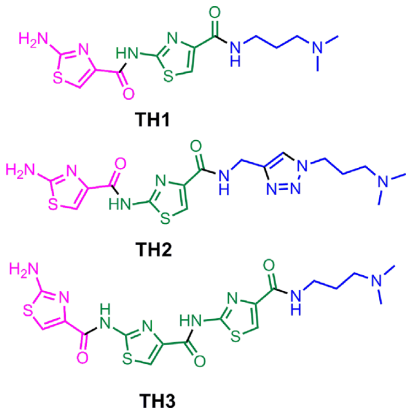

Figure 1. Structure of thiazole peptides (**TH 1–3**).

zole peptides with G-quadruplexes has been investigated using Förster resonance energy transfer (FRET) melting analysis, fluorescence and NMR spectroscopic studies. Our results show that one molecule of thiazole peptide **TH3** interacts with each of the terminal G-quartets and capping structures of 5′- and 3′-ends of *c-MYC* G-quadruplex. Subsequently, the downstream effect of **TH3** has been investigated in human cancer cells using XTT assay, quantitative real time PCR (qRT-PCR), Western blotting, dual luciferase and flow cytometric assay.

MATERIALS AND METHODS

General materials

The general chemicals and labeled DNA sequences were purchased from Sigma-Aldrich. The detailed description of materials used in synthesis has been described in the supporting information section. The labeled DNA sequences of highest purity were purchased for best results. The typical cell culture reagents and the antibodies were purchased from Thermo Fisher Scientific and Merck Millipore, unless stated otherwise. The Annexin V-FITC kit for apoptosis assay was purchased from Life technologies. The *c-MYC* promoter (Del4) was a gift from Bert Vogelstein (Addgene plasmid # 16604). The *BCL-2* luciferase plasmid LB322 (*BCL-2* from ATG to –3934) was a gift from Linda Boxer (Addgene plasmid # 15381). The renilla luciferase plasmid pRL-TK was a gift from Dr Susanta Roychoudhury, Indian Institute of Chemical Biology, Kolkata. The dual luciferase reporter assay kit was purchased from Promega.

Synthesis of thiazole peptides

Thiazole peptides (Figure 1) were synthesized using sequential amide bond formation and outlined in Schemes S1-S7 (Supplementary Information). The detailed synthesis and characterization are described in the supplementary information.

FRET melting analysis

FRET melting assay using ligands **TH1**–**TH3** were carried out in a 96-well format on a real-time PCR apparatus (Roche LightCycler® 480 II) (24). Dual labeled DNA sequences with a donor fluorophore 6-carboxyfluorescein (5′-FAM) and an acceptor fluorophore 6-carboxytetramethylrhodamine (3′-TAMRA) were used for the study.

- *c-MYC*14/23: 5′ FAM-d(TGAG$_3$TG$_3$TAG$_3$TG$_3$TA$_2$)-TAMRA 3′
- *c-MYC*Pu27*:* 5′ FAM-d(TG$_4$AG$_3$TG$_4$AG$_3$TG$_4$A$_2$G$_2$TG$_4$A)-TAMRA 3′
- *c-KIT1:* 5′ FAM-d(G$_3$AG$_3$CGCTG$_3$AG$_2$AG$_3$)-TAMRA 3′
- *c-KIT2*: 5′ FAM-d(G$_3$CG$_3$CGCTAG$_3$AG$_4$)-TAMRA 3′
- *BCL-2*: 5′ FAM-d(G$_3$CGCG$_3$AG$_2$A$_2$T$_2$G$_3$CG$_3$)-TAMRA 3′
- hairpin DNA: 5′ FAM-d(TATAGCTATA$_8$TATAGCTATA)-TAMRA 3′
- ds26: 5′-d(CA$_2$TCG$_2$ATCGA$_2$T$_2$CGATC$_2$GAT$_2$G)-3′

200 μM stock solutions of peptides **TH1**–**TH3** were prepared in 60 mM potassium cacodylate buffer, or 100 mM KCl, 10 mM Tris•HCl buffer, pH 7.4. Dual labeled oligos were diluted from stock to a concentration of 400 nM in the same buffer. The diluted samples were annealed by heating to 95°C for 5 min followed by gradual cooling at 25°C and incubated overnight at 4°C. Sample solutions were prepared in a 96-well plate (100 μl final volume) by mixing pre-annealed DNA (at 200 nM final concentration) with peptides (1.0 μM final concentration) in respective buffer (60 mM potassium cacodylate, or 100 mM KCl, 10 mM Tris•HCl buffer, pH 7.4). After 1 h incubation, measurements were made in triplicate with excitation at 483 nm and detection at 533 nm. Final analysis of the data was carried out using OriginPro 8.0 (OriginLab Corp.). The detailed procedure for FRET analysis has been included in the supplementary information.

Fluorimetric titration

Fluorescence spectra were recorded on a Horiba JobinYvon Fluorolog instrument at 25°C in a thermostated cell holder using quartz cuvette of 1 cm path-length. The DNA sequences used in the study are described in the supplementary information. Briefly, DNA sequences were pre-annealed in Tris–KCl buffer (100 mM KCl, 10 mM Tris•HCl, pH 7.4). Peptides (**TH1**, **TH2** and **TH3**) were diluted in filtered and degassed Tris-KCl buffer to a final concentration of 2 μM. Peptide solutions were titrated with the pre-annealed DNA sequences and the emission was recorded from the range of 315–600 nm (λ_{ex} = 300 nm). The recorded spectral data was used to determine the dissociation constant of the ligands for quadruplexes using the Hill-1 formula:

$$F = F_0 + \frac{(F_{max} - F_0)[DNA]}{K_d + [DNA]}$$

F is the fluorescence intensity, F_{max} is the maximum fluorescence intensity, F_0 is the fluorescence intensity in the absence of DNA and K_d is the dissociation constant.

NMR titration

The *c-MYC* DNA (*c-MYC*14/23 and *c-MYC*Pu27) was purchased from Eurofins MWG Operon in HPSF purity grade and further purified with HPLC. During the titration the DNA was provided as a 100 μM solution in 25 mM Tris•HCl buffer (pH 7.4) with 100 mM KCl in 10% d_6-DMSO/90% H_2O. Small amounts of the ligand stock solution in 100% d_6-DMSO were added directly into the NMR tube (12.8% d_6-DMSO at the end of the titration). 2,2-dimethyl-2-silapentane-5-sulphonate (DSS) was used as internal reference. Watergate W5 pulse sequence with gradients (25) or jump-return-Echo (26) was used for water suppression. 2D NMR experiments were recorded on the DNA alone (1 mM) and in the complex with 3 equivalents of ligand in 25 mM potassium phosphate pH 7.0 containing 70 mM KCl in 10% d_6-DMSO/90% H_2O to reduce the conformational diversity according to Yang *et al.* (10) and to avoid loss of sensitivity due to Tris signal. ^1H,^{13}C HSQC (27,28) spectra and 2D ^1H,^1H NOESY spectra with excitation sculpting as water suppression scheme (29) were recorded.

Cell culture

Human cervical cancer cells (HeLa) and human alveolar basal epithelial cancer cells (A549) were obtained as monolayer culture from the National Centre for Cell Science (NCCS), Pune and cultured in Dulbecco's Modified Eagle Medium (DMEM) supplemented with D-glucose, L-glutamine, penicillin–streptomycin (Invitrogen) and 10% fetal bovine serum (Gibco). HeLa cells were seeded in 6-well plates at a concentration of 1×10^5 cells per well and incubated at 37°C in 5% CO_2 incubator to obtain >70% confluency before treatment. Then the cells were treated with ligands and incubated under the same conditions for another 24 h and were harvested for further analysis.

Cell cytotoxicity assay

Cancer Cells (HeLa and A549) and Normal Kidney Epithelial (NKE) were seeded in a 96-well plates (1×10^3 cells/well) and exposed to various concentrations of peptides **TH2** and **TH3** (Control, 0.5, 1.0, 2.0, 4.0, 5.0, 10.0, 15.0, 20.0, 40.0, 60.0, 80.0 and 100.0 μM). XTT (2,3-bis-(2-methoxy-4-nitro-5-sulfophenyl)-2H-tetrazolium-5-carboxanilide) (Thermo Fisher Scientific) stock solution was prepared by mixing 4 ml (1 mg/ml) with 10 μl of the 10 mM phenazine methosulfate (PMS) (Thermo Fisher Scientific) solution. After 24 h treatment with peptide ligands, 25 μl of XTT/PMS stock solution was added to each well and further incubated for 2 h at 37°C. The absorbance was directly recorded at 450 nm by an automated microplate reader (Thermo Fisher Scientific). All experiments were performed in parallel and in triplicate, and the IC_{50} values were derived from the linear regression parameters using OriginPro 8.0 (OriginLab Corp.).

RNA extraction and qRT-PCR

After HeLa and A549 cells were treated with peptides **TH2** and **TH3** (2.0 and 5.0 μM) for 24 h, the total RNA was extracted using TRIzol reagent (Invitrogen) according to the manufacturer's protocol. The RNA was quantitated using a Cary Win 300 UV-Vis spectrophotometer and the total RNA was used as a template for reverse transcription using a Verso cDNA synthesis kit (Thermo Fisher Scientific) according to the protocol supplied. The mixtures were incubated at 42°C for 30 min for reverse transcription and then at 95°C for 2 min followed by incubation at 4°C. Afterward, PCR reactions were performed in a Light Cycler® 480 II (Roche) apparatus. A total volume of 20 μl qRT-PCR reaction mixture was prepared containing 10 μl of SYBR green Jump Start Taq Ready Mix (Sigma) reagent, 1 μl each of the forward and reverse primers (500 nM), 2 μl of cDNA (200 nM) and nuclease-free water to make up the volume. Cycle conditions were as follows: pre-incubation at 95°C for 10 min, followed by 40 cycles of 95°C for 15 s, 60°C for 60 s, then hold at 37°C for 2 min. The primer sequences used for qRT-PCR are:

- GAPDH (forward): 5′-$GACG_2C_2GCATCT_2CT_2GT$-3′
- GAPDH (reverse): 5′-$CACAC_2GAC_2T_2CAC_2AT_4$-3′
- 18S rRNA (forward): 5′-$GAT_2C_2GTG_3TG_2TG_2TGC$-3′
- 18S rRNA (reverse): 5′-$A_2GA_2GT_2G_5ACGC_2GA$-3′
- *c-MYC* (forward): 5′-$CTGCGACGAG_2AG_2AG_2AC$T-3′
- *c-MYC* (reverse): 5′- $G_2CAGCAGCTCGA_2T_3CT_2$-3′
- *BCL-2* (forward): 5′-$GAG_2AT_2GTG_2C_2T_2CT_3G$-3′
- *BCL-2* (reverse): 5′-$GC_2G_2T_2CAG_2TACTCAGTC$-3′

We used the comparative cycle threshold method (C_T method) for relative quantification of gene expression. Further details have been included in supplementary information.

Western blot analysis

HeLa cells were treated with peptide ligands **TH2** and **TH3** (2.0 and 5.0 μM) for 24 h and subsequently, cells were lysed with cold cell lysis buffer (25 mM Tris, 150 mM NaCl, 1 mM EDTA in 1% Triton X-100 and 5% glycerol). Cell lysates were collected and the total protein content was estimated by the Lowry method (30). An aliquot of 70 μg of protein extract was loaded in each lane and separated in a 10% SDS-PAGE gel and electroblotted in 48 mM Tris, 39 mM Glycine, 20% methanol and 0.02% SDS on a nitrocellulose transfer membrane. Membrane was then blocked with 4% BSA in 1× TBS and 0.1% TWEEN®20, washed and probed using antibodies directed against *c-MYC, BCL-2* and GAPDH (endogenous loading control) overnight at room temperature. Blots were then washed and incubated with (i) 1:2000 dilution of ALKP conjugated secondary antibody (for *c-MYC*) (Life technologies), (ii) 1:2000 dilution of HRP secondary antibody (for GAPDH) (Life technologies) and (iii) 1:2000 dilution of HRP secondary antibody (for *BCL-2*) for 2 h at room temperature. Binding signals were visualized with NBD/BCIP substrate. Relative band intensities were determined by using ImageJ software.

In situ mutagenesis, transfection and dual luciferase assay

The Del4 luciferase reporter plasmid (Addgene plasmid # 16604) was mutagenized by using the Quick Change Site

directed Mutagenesis kit (Agilent Technologies, CA, USA) with the following primers:

- Forward: 5′-TGAG$_4$CG$_2$AGCTG$_2$C$_2$GCACG$_3$AGA-3′
- Reverse: 5′-TCTC$_3$GTGCG$_2$C$_2$AGCTC$_2$GC$_4$TCA-3′

Exponentially growing HeLa cells in DMEM media supplemented with 10% FBS were seeded in a six-well plate. The plasmid used for transfection was Del4 which harbors the 22-mer *c-MYC* G4 forming sequence in the P1 promoter upstream of the luciferase reporter (Addgene). Del4 mutant plasmid containing mutated G4-forming sequence was used as control. The G4 forming sequences upstream of luciferase reporter gene in the plasmids used in the current study are as following:

- Del4: 5′-G$_4$AG$_3$TG$_4$AG$_3$TG$_4$-3′
- Mut-Del4: 5′-G$_4$AG$_3$TGAG$_2$AG$_3$TG$_4$-3′ (substitution is underlined)

500 ng plasmid was transfected in HeLa cells growing at >70% confluency using Lipofectamine 2000 as per manufacture's protocol. After 6 h of transfection, cells were washed with PBS and fresh media was added. Cells were treated with peptides **TH2** and **TH3** (2.0 and 5.0 μM) for 24 h. Then cells were lysed with Cell Culture Lysis Reagent (CCLR) buffer with continuous pipetting at 48°C for 30 min. The homogenate was centrifuged for 5 min at 10,000 g. The supernatant is used for protein estimation by Lowry method (30). Luciferase assay was performed in Orion Microplate Luminometer (Berthold Detection System) for three biological replicates and luciferase activity was normalized by total protein concentration.

Cell cycle analysis

Cell cycle analysis was carried out using propidium iodide (PI) staining by flow cytometry. HeLa cells (1×10^6) per 60 mm petridish (∼80% confluence) were treated with **TH3** (2.0 and 5.0 μM) for 24 h in fresh growth medium. Cells were harvested by trypsinization, resuspended in PBS and fixed with 2 ml of ice-cold 70% ethanol for overnight at 4°C. The pellets were collected by centrifugation and resuspended in PBS solution, containing 10 μg/ml PI (Sigma) and 10 μg/ml RNase A (Sigma). After incubation for 30 min in the dark at 37°C, cells were analyzed for DNA content using a FACS flow cytometer (BD Biosciences). Cell distribution among cell cycle phases were evaluated using Cell-Quest Pro software (BD).

Flow cytometric determination of apoptosis

Annexin V–FITC and propidium iodide (PI) were used to determine the percentage of cells undergo apoptosis and necrosis. Briefly, 1×10^6 HeLa cells per 60 mm Petridish (∼80% confluence) were treated with peptide **TH3** (2.0 and 5.0 μM) for 24 h in fresh growth medium. Cells were harvested with trypsinization and centrifuged at 700 rpm for 5 min at 4°C. Cell pellet was suspended in 500 μl 1× binding buffer and then treated with 5 μl Annexin V–FITC and 2 μl PI. After incubation for 5 min on ice, each sample was analyzed immediately using fluorescence-activated cell sorter (FACS) analysis (BD Biosciences,Mountain View, CA, USA). Approximately 10 000 HeLa cells were detected for each sample. Cytogram analysis was done using the Cell-Quest Pro software.

Fluorescence microscopy

Cellular localization of thiazole peptide **TH3** was monitored by cell imaging. HeLa cells were seeded on glass cover slips placed in 12-well cell culture plates for 24 h followed by incubation with **TH3** (5.0 μM) for 2 h in CO_2 (5%) incubator at 37°C. After incubation, cells were washed with PBS buffer three times and the cover slips were mounted on glass slides using NucRed (1:1 solution in PBS) and localization of **TH3** was viewed under (Olympus IX 81 Confocal Laser Scanning Microscope). At least five fields per slide and three independent sets were examined.

RESULT AND DISCUSSION

Design of thiazole peptides

The five-membered thiazole heterocycle, derived by enzyme-mediated post-translational modification (31–33) of natural amino acid residues is present in numerous cyclic peptides (34–39) that exhibit pharmaceutically useful biological activities. The thiazole moiety is also present in antitumor drugs like bleomycin and tiazofurin (40). Telomestatin, one of the potent G-quadruplex binding ligands contains seven oxazole rings and one thiazoline ring system (41). Inspired from Telomestatin, numerous oxazole macrocycles have been developed for targeting DNA G-quadruplexes (39,42,43). The observation that the triazole containing distamycin and netropsin interacts with DNA minor groove by hydrophobic interaction has led to the development of other selective DNA groove targeting ligands (35). However, distamycin has also been reported to bind to G-quadruplex by specific stacking interaction with terminal G-quartets (44). Interestingly, a 4:1 (ligand:DNA) stoichiometry was reported in both models.

We have anticipated that thiazole peptides, capable of adopting crescent shape, may selectively interact with a particular G-quadruplex. The detailed synthesis of the thiazole peptides (**TH 1-3**) has been described in the supporting information (Figure 1 and Supplementary Figure S1, Scheme S1–S7). Peptide **TH1** contains two thiazole rings whereas peptide **TH2** contains two thiazole rings and a triazole ring. In peptide **TH3**, three thiazole rings are connected through amide bonding. To understand the difference in three dimensional structure of **TH2** and **TH3**, energy minimized structures of **TH2** and **TH3** were obtained with Gaussian 03 using DFT (Density functional theory) analysis B3LYP/6-31+G(d) level (Supplementary Figures S2 and S3). Unlike **TH2**, the HOMO (highest occupied molecular orbital) and LUMO (lowest unoccupied molecular orbital) orbitals of **TH3** are non-overlapping, distributed over a larger area. Therefore, effective conjugation of π-electrons is expected in peptide **TH3**. On the other hand, the presence of an additional –CH_2 linker between thiazole and triazole moieties in peptide **TH2** inhibits the π-electron delocalization and provides flexibility to form distorted structure. In comparison, **TH3** exists in planar crescent shape as the pep-

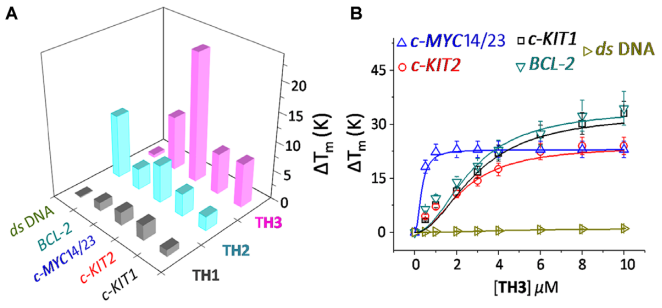

Figure 2. (**A**) Stabilization potential (ΔT_m) of the ligands **TH1**, **TH2** and **TH3** for G-quadruplex and hairpin DNA by FRET melting assay; (**B**) Thermal shift profiles of **TH3** upon interacting with quadruplexes and hairpin DNA in 60 mM K^+-cacodylate buffer, pH 7.4.

tide linkages are less flexible due to their partial double bond character and able to mediate effective π-conjugation. The HOMO-LUMO energy difference values, calculated for peptides **TH2** and **TH3** were 6.8 and 6.5 eV, respectively. In this study, thiazole peptides (**TH 1–3**) having different length and three dimensional structures have been investigated as G-quadruplex targeting ligands for chemical regulation of oncogene expression and anticancer therapeutics.

Quadruplex specificity of thiazole peptides

The ability of thiazole peptides to distinguish between quadruplexes was examined by FRET melting assay and fluorimetric titration experiments. We have used four different intramolecular quadruplexes like *c-MYC*, *c-KIT1*, *c-KIT2* and *BCL-2*, a control hairpin DNA and a self complementary duplex DNA (ds26). For the *c-MYC*, we have used a wild-type 27-mer *c-MYC*Pu27 sequence as well as a 22-mer *c-MYC*14/23 conformer that contains two G-to-T mutations at 14 and 23 positions of the *c-MYC*Pu27 sequence (10).

FRET melting assay. FRET melting analysis was employed to evaluate the ability of thiazole peptides (**TH1-TH3**) to stabilize the dual labeled (FAM and TAMRA at 5′- and 3′-ends, respectively) G-quadruplexes (*c-MYC*, *c-KIT1*, *c-KIT2* and *BCL-2*) and a control hairpin DNA (Figure 2A) (24). The dipeptide **TH1** (1.0 μM, 5.0 equiv.) displayed negligible stabilization potential values for G-quadruplexes and hairpin DNA. Although the dipeptide **TH2** (1.0 μM, 5.0 equiv.) containing a triazole moiety showed low ΔT_m values (2–6°C) for quadruplexes, it could increase the melting temperature of hairpin DNA ($\Delta T_m = 11$°C) (Figure 2, Table 1, Supplementary Table S1). Tripeptide **TH3** exhibited a high stabilization potential for the *c-MYC*14/23 G-quadruplex ($\Delta T_m = 22$°C) compared to dipeptides **TH1** and **TH2** at 1.0 μM ligand concentration (5.0 equiv. with respect to DNA). It is further interesting to note that **TH3** (1.0 μM, 5.0 equiv.) could preferentially stabilize the *c-MYC*14/23 G-quadruplex ($\Delta T_m \sim 22$°C) over the *c-KIT1*, *c-KIT2*, and *BCL-2* quadruplexes ($\Delta T_m \sim 7 - 9$°C). In addition, **TH3** did not alter the T_m value of hairpin DNA.

Next, the FRET melting analysis of promoter quadruplexes and hairpin DNA was carried out with incremental addition of **TH3** (0–10 μM) (Figure 2B). A maximum ΔT_m value of 22 ± 1°C (i.e. a T_m of 92°C) was observed for the *c-MYC*14/23 in the presence of 1.0 μM **TH3** (Figure 2B), whereas 5–7 fold higher concentrations of **TH3** was required to attain similar ΔT_m values ($\Delta T_m = 22$°C) for *c-KIT1, c-KIT2* and *BCL-2* suggesting its high affinity towards the *c-MYC*14/23 quadruplex. **TH3** (1.0 μM) could stabilize *c-MYC*Pu27 with a ΔT_m value of 21 ± 1°C (i.e. a T_m of 91°C) (Supplementary Figure S4). In addition, peptide **TH3** does not significantly alter the melting temperature of hairpin DNA even at 10.0 μM ligand concentration (50.0 equiv.).

A FRET competitive experiment was performed to evaluate the selectivity of **TH3** for the *c-MYC* G-quadruplex over double stranded DNA (Supplementary Figure S5). The melting of 200 nM dual labeled *c-MYC*14/23 was carried out with **TH3** (1 μM) in the presence of a competitor ds26 DNA. The results indicated that the ΔT_m value of **TH3** for the *c-MYC*14/23 G-quadruplex was not significantly decreased by adding excess of ds26 DNA, at ds26/*c-MYC*14/23 ratios up to 50/1 (Supplementary Figure S5).

Fluorimetric titrations. The interaction of thiazole peptides with G-quadruplexes (*c-MYC, BCL-2, c-KIT1* and *c-KIT2*) and ds26 (Figure 3) was investigated using fluorescence spectroscopy. Peptides **TH1**, **TH2** and **TH3** exhibited a single broad band with an emission maximum at 430 nm, when excited at 300 nm ($\lambda_{abs} = 300$ nm) in buffer solution (10 mM Tris•HCl, 100 mM KCl, pH 7.4) (Figure 3, Supplementary Figures S6–S10). The binding of **TH3** to the *c-MYC*14/23 quadruplex resulted in ∼6-fold intensification of the fluorescence at saturation. In contrast, small changes in the fluorescence intensity of **TH1** and **TH2** were observed upon the addition of DNA quadruplexes. These changes in fluorescence were used to determine affinities for the binding of the peptides to quadruplexes. The dissociation constant (K_d) of ligand **TH3** is 0.25 μM for the *c-MYC*14/23 quadruplex while **TH1** and **TH2** exhibited K_d values of 4.81 μM and 2.82 μM for the *c-MYC*14/23 G-quadruplex, respectively. **TH3** also binds to *c-MYC*Pu27 ($K_d = 0.29$ μM) with comparable affinity as *c-MYC*14/23 (Supplementary Figure S11). These results indicate that **TH3** displays strong binding for the *c-MYC* G-quadruplex with ∼19- and ∼11-fold higher binding affinity compared to **TH1** and **TH2**, respectively. Similar binding titrations with other promoter quadruplexes indicated ∼4–5-fold selectivity of **TH3** for the *c-MYC* G-quadruplex ($K_d \sim 0.25$ μM) over *c-KIT1, c-KIT2* and *BCL-2* quadruplexes ($K_d \sim 1.17$–1.34 μM) (Figure 3, Table 1). The Job's plot analysis revealed that the **TH3** binds to the *c-MYC*14/23 G-quadruplex with a 2:1 stoichiometry (Supplementary Figure S12).

Moreover, ligands **TH1** and **TH3** exhibited negligible changes in fluorescence intensities upon addition of 4 equiv. ds26 duplex DNA. However, an increase in fluorescence intensity of **TH2** was observed in the presence of ds26 ($K_d = 0.9$ μM) indicating its high binding affinity for the ds26. These results indicate that thiazole tripeptide **TH3** binds more strongly to quadruplexes than dipeptides **TH1** and **TH2**. Furthermore, **TH3** binds to the *c-MYC* with high specificity over other quadruplexes and ds26.

Table 1. Sequences used in this study and binding data obtained from FRET melting (ΔT_m) and fluorescence studies (K_d)

	TH1		TH2		TH3	
DNA[a]	ΔT_m[b]	K_d[c]	ΔT_m[b]	K_d[c]	ΔT_m[b]	K_d[c]
*c-MYC*14/23: 5′-d($TGAG_3TG_3TAG_3TG_3TA_2$)-3′	2.5	4.81	6.5	2.82	22.0	0.25
c-KIT1: 5′-d($G_3AG_3CGCTG_3AG_2AG_3$)-3′	1.4	5.15	3.7	3.27	9.5	1.17
c-KIT2: 5′-d($G_3CG_3CGCTAG_3AG_4$)-3′	1.1	20.52	2.5	3.53	7.6	1.34
BCL-2: 5′-d(GGGCGCGGGAGGAATTGGGCGGG)-3′	2.0	9.81	3.9	4.01	7.1	1.22
ds DNA: 5′-d($TATAGCTATA_8TATAGCTATA$)-3′	1.0	n.d	11.0	0.90	2.0	n.d.

[a]The T_m values of the quadruplexes in 60 mM potassium cacodylate buffer, pH 7.4 in the absence of ligands are: *c-MYC*14/23 (70±1), *BCL-2* (70±1), *c-KIT1* (57±1), *c-KIT2* (69±1), *ds* DNA (60±1) °C; maximum measurable T_m = 93 °C. Dual FAM-TAMRA labeled sequences were used in the FRET melting experiments.
[b]ΔT_m at 1 μM ligand concentration [°C] ($\Delta T_m = \pm 1$°C).
[c]$K_d = \pm 10\%$ (expressed in μM).

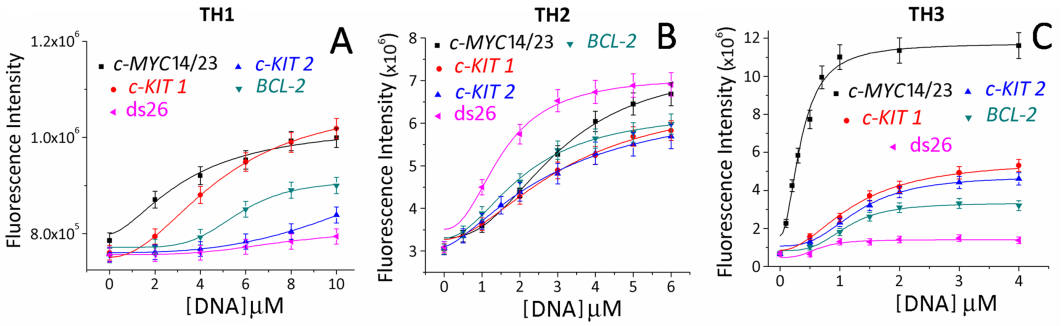

Figure 3. Fluorescence titration of (**A**) **TH1** (2 μM) with *c-MYC*14/23, *c-KIT1*, *c-KIT2*, *BCL*-2 and ds26 (0–10 equiv.), (**B**) **TH2** (2 μM) with *c-MYC*14/23, *c-KIT1*, *c-KIT2*, *BCL*-2 and ds26 (0–6 equiv.) and (**C**) **TH3** (2 μM) with *c-MYC*14/23, *c-KIT1*, *c-KIT2*, *BCL*-2 and ds26 (0–4 equiv.).

Binding mode of TH3 with *c-MYC* G-quadruplex

NMR titrations. The interaction of **TH3** with *c-MYC*14/23 (45) and the *c-MYC*Pu27 (45) (Supplementary Figure S13) (Figure 4) was investigated by recording 1D ^{1}H NMR spectra at different [**TH3**]:[DNA] ratios. The titrations were performed in 10% d_6-DMSO/90% H_2O due to low solubility of the peptide **TH3** in NMR buffer (Supplementary Figures S14 and S15). The sequence *c-MYC*Pu27 is known to form a mixture of G-quadruplex conformations with different loops (45) and the imino pattern in the 1D ^{1}H NMR spectrum is very broad and not suitable for a detailed NMR assignment. Only minor changes could be observed on the 1D ^{1}H NMR spectrum of *c-MYC*Pu27 DNA after ligand addition and none of the various conformations seemed to be stabilized by **TH3** (Supplementary Figure S13). The *c-MYC*14/23 G-quadruplex mutant forms a defined G-quadruplex structure that has been characterized by Yang *et al.* (PDB: 1XAV) (10). The effect of DMSO on the G-quadruplex formed by the sequence *c-MYC*14/23 G-quadruplex has been previously discussed (46) and the assignment for the target DNA has been transferred from Yang *et al.* (10,11). Clear changes in the 1D ^{1}H spectrum upon addition of the ligand to the G-quadruplex formed by the sequence *c-MYC*14/23 were detected. Upon addition of 0.25 eq. of **TH3**, strong line broadening was observed for all the imino signals (Figure 4A) as well as for most aromatic signals (Figure 4B). At a [**TH3**]:[DNA] ratio of 2:1, a new set of imino proton signals appeared (Figure 4A), suggesting that the ligand is binding to the DNA with a 2:1 stoichiometry in slow exchange on the NMR time scale. With further addition of ligand, the imino signals became sharper.

In the literature, different binding modes to G-quadruplex have been proposed for distamycin A, structurally related to **TH3**. Maizels and co-workers observed a 4:1 stoichiometry with two molecules binding to each of the two external tetrads (44). Randazzo and co-workers reported that distamycin A binds as a dimer to the grooves of a tetramolecular G-quadruplex with a 4:1 stoichiometry (47,48).

CSP analysis. In order to gain an insight into the binding mode of **TH3**, 2D ^{1}H, ^{1}H-NOESY and 2D ^{1}H, ^{13}C-HSQC have been recorded for the assignment of the G-quadruplex in complex with **TH3** (Supplementary Figures S18–S19). However, the signals of the ligand in the bound form could not be detected and no NOE intermolecular crosspeaks could be observed under the experimental conditions used in our studies. Therefore, the chemical shift perturbations (CSPs) after ligand binding have been analyzed in detail. The assignment of the complex used for CSP calculation (Supplementary Equation S2) is shown in Figure 5A with black labels, while the assignment of the G-quadruplex alone is in gray labels. The combined CSPs (Supplementary Table S4) of the imino protons (H1, Supplementary Figure S19, Supplementary Table S2) and of the anomeric (C1′H1′, Supplementary Figure S18A, Supplementary Table S3) and aromatic (C8/C6, H8/H6, Supplementary Figure S18B, Supplementary Table S3) signals are displayed as bar chart in Supplementary Figure S20 and on the structure of *c-MYC*14/23 (Figure 5B and Supple-

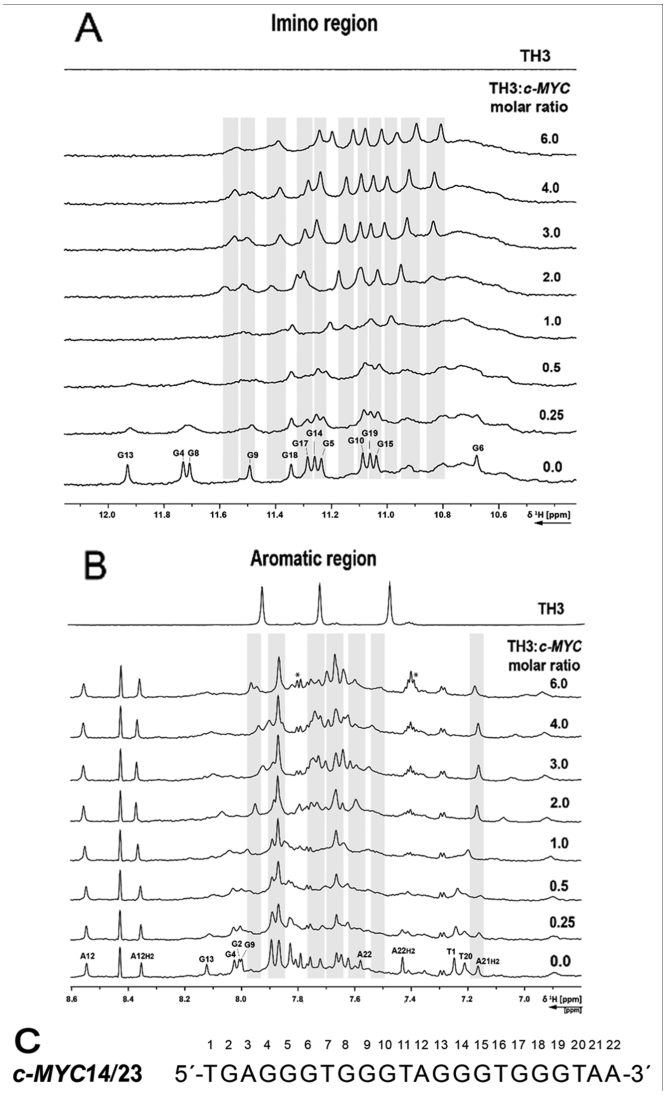

Figure 4. (**A**) Imino and (**B**) aromatic region of 1D ^{1}H NMR spectrum of the *c-MYC*14/23 G-quadruplex DNA with increasing [**TH3**]:[DNA] ratio and ligand alone. The spectra were recorded at 298 K, 700 MHz. Experimental conditions: 100 μM DNA in 25 mM Tris•HCl (pH 7.4) buffer containing 100 mM KCl in 10% d_6-DMSO/90% H_2O. (**C**) Sequence of *c-MYC*14/23 with the numbering used for the partial assignment of DNA signals. Signals marked with a star are arising from ligand self-aggregation (∼10%, Supplementary Figure S16) after transferring in buffer during the titration. These aggregated species do not interact with the DNA (Supplementary Figure S17)

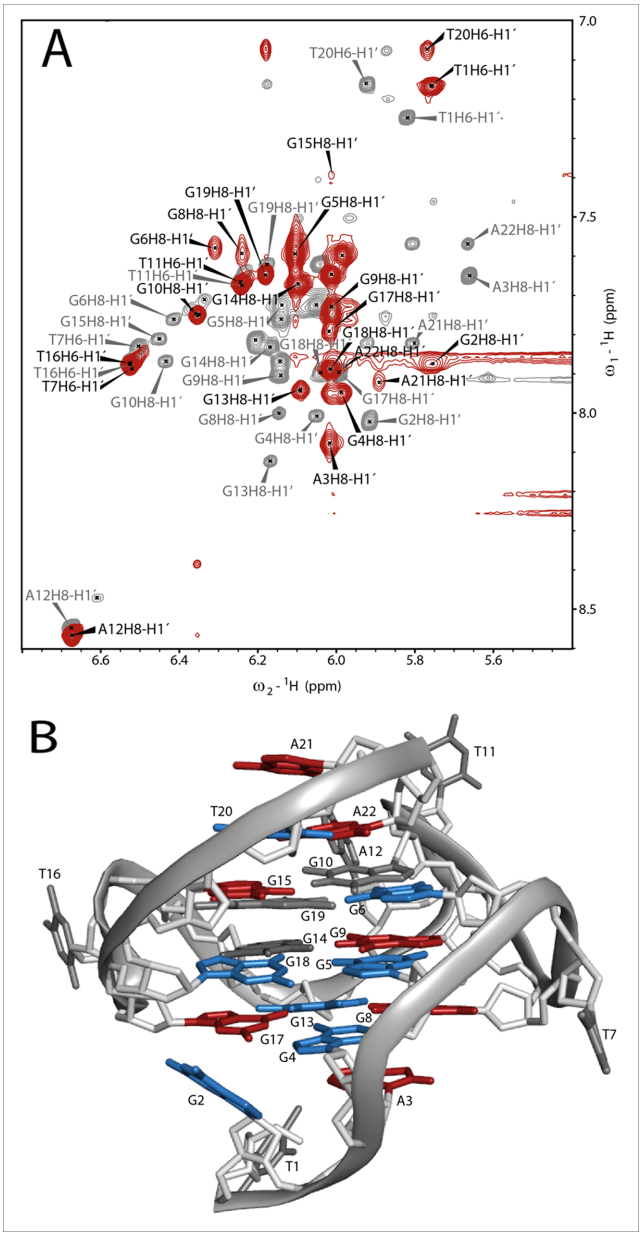

Figure 5. (**A**) Overlay of the H1′H6/H1′H8 region of the ^{1}H,^{1}H-NOESYs of *c-MYC*14/23 (gray) and the complex (red). The assignment of *c-MYC*14/23 (gray labels) has been transferred from Yang *et al.* (10). The attempt of assignment of the signals for the complex (black labels) is based on the analysis of ^{1}H,^{13}C-HSQC (Supplementary Figure S18) and the ^{1}H,^{1}H-NOESY spectra. In the overlay it is already possible to estimate qualitatively the strength of chemical shift perturbation (CSP) of the anomeric (H1′) and aromatic (H6/H8) protons after ligand binding. Experimental conditions: 298 K, 25 mM potassium phosphate pH 7.0, 70 mM KCl, 10% d6-DMSO,1 mM DNA (gray spectrum) and 1 mM DNA with 3 eq. of **TH3.** (**B**) Structure of *c-MYC*14/23 (PDB: 1XAV) with colored nucleobases according to their combined CSP after ligand binding with residue numbering according to Figure 4C. Gray: non shifted (CSP ≤ 0.1), blue: moderately shifted (CSP = 0.1 – 0.2) and red: strongly shifted (CSP > 0.2).

mentary Figure S21A), where the nucleobases were colored according to three different categories: non or hardly shifted (CSP ≤ 0.1, gray), moderately shifted (CSP = 0.1–0.2, blue) and strongly shifted (CSP > 0.2, red).

The nucleobases with the strongest CSP (red color code) are located at the 3′- and 5′-ends (A3, G8, G15, G17, A21 and A22) of the G-quadruplex structure. The lack of ligand signals in the bound state does not allow us to determine whether the ligand interacts with the 3′- and 5′-capping structures, with the terminal G-quartets or it is sandwiched between both of them. According to the CSP analysis together with the titration monitored by 1D ^{1}H spectra point-

ing at a complex with a 2:1 [**TH3**]:[DNA] ratio, we propose that one ligand molecule is binding at the 3′-end and the other one at the 5′-end. This binding mode is comparable with the one observed by Maizels and co-workers (44), although they reported a different binding stoichiometry. We did not observe induced CD (circular dichroism) signals upon titrating *c-MYC*14/23 with **TH3**, which suggests that ligand does not bind to the G-quadruplex grooves as observed in case of distamycin A by Randazzo and coworkers (Supplementary Figure S22).

Structure-activity relationship

The differences in 3D structures of peptides **TH 1-3** may provide the rationale behind their differential affinity towards different G-quadruplexes. Out of these three peptides, only **TH3** exist in planar crescent structure due to extended π-electron conjugation between three thiazole moieties (Supplementary Figure S3). Owing to the lack of extended π-electron conjugation in **TH1** (only two thiazole moieties present) and **TH2** (additional $-CH_2$ present between thiazole and triazole moieties), they do not exhibit the planar crescent structure. As a result, their recognition sites in a G-quadruplex structure is expected to be different.

Although the G-quadruplex structures (*c-MYC*14/23, *c-KIT1*, *c-KIT2* and *BCL-2*), used in this study exist in parallel topology, the intermediate loop sequences and flanking regions (capping structures) are quite different (Supplementary Figure S21). A close inspection of these structures indicates that *c-MYC*14/23 G-quadruplex contains AT-rich capping structures at both 5′ and 3′ ends, which are absent or truncated in other G-quadruplexes. The presence of extended planar structure of **TH3** promotes higher stacking interaction with the terminal G-quartets compared to **TH1** and **TH2**. In addition, the NMR analysis shows that the peptide **TH3** interacts with the AT-rich 5′ and 3′ ends of *c-MYC* G-quadruplex structure. These capping structures are unique in *c-MYC* G-quadruplex structure, which may be the reason for the observed selectivity of peptide **TH3** towards *c-MYC* G-quadruplex over other G-quadruplexes.

Ligand dependent *c-MYC* expression in cancer cells

Since **TH3** was found to be a selective ligand for targeting *c-MYC* G-quadruplex structure over other promoter G-quadruplexes, the influence of **TH3** on the *c-MYC* gene expression was evaluated using qRT-PCR analysis, western blot and dual-luciferase assay. For a comparison, the influence of a less potent G-quadruplex binder, **TH2** on the *c-MYC* gene expression was also investigated.

qRT-PCR analysis. The effect of ligands **TH2** and **TH3** on *c-MYC* transcription was investigated by monitoring the mRNA expression profiles in human cervical cancer cells (HeLa) cells (Figure 6A, B and Supplementary Figure S23). Cells were treated with various concentrations (2.0 and 5.0 μM) of **TH2** and **TH3** for 24 h, and the expression of *c-MYC* mRNA was normalized against the constitutively expressed housekeeping gene, glyceraldehyde-3-phosphate dehydrogenase (GAPDH). **TH3** reduced the *c-MYC* mRNA level to 0.3-fold (decreased by 70% relative

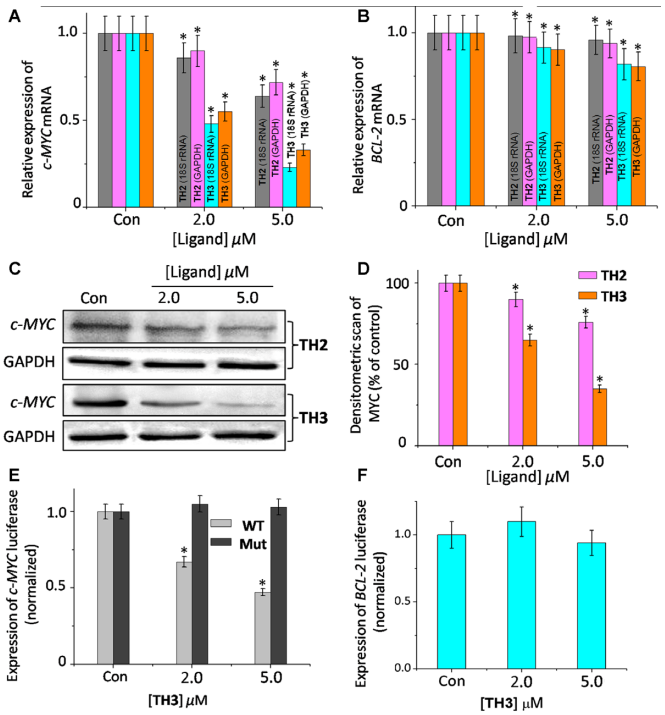

Figure 6. Determination of transcriptional regulation of (**A**) *c-MYC* mRNA, (**B**) *BCL-2* mRNA in the presence of **TH2** and **TH3** in cancer cells (HeLa) by qRT-PCR and quantified by double delta C_t analysis using 18S rRNA and GAPDH as reference genes. Data is presented in terms of fold change. Data shown as mean ± SD. $^*P < 0.05$, versus untreated cancer cells; (**C**) immunoreactive bands of *c-MYC* protein were analyzed by Western blot in HeLa cells. Data shown as mean ± SD. $^*P < 0.05$, versus untreated cancer cells; (**D**) the protein expression of *c-MYC* protein in the presence of **TH2** and **TH3** in HeLa cells. Relative luciferase expression in (**E**) Del4 *c-MYC*/mut-*c-MYC* and (**F**) LB322 *BCL-2* promoter containing firefly plasmid normalized with pRL-TK Renilla plasmid (FF/RL) upon treatment of **TH3** in HeLa cells, Data shown as mean ± SD. $^*P < 0.05$, versus untreated cancer cells.

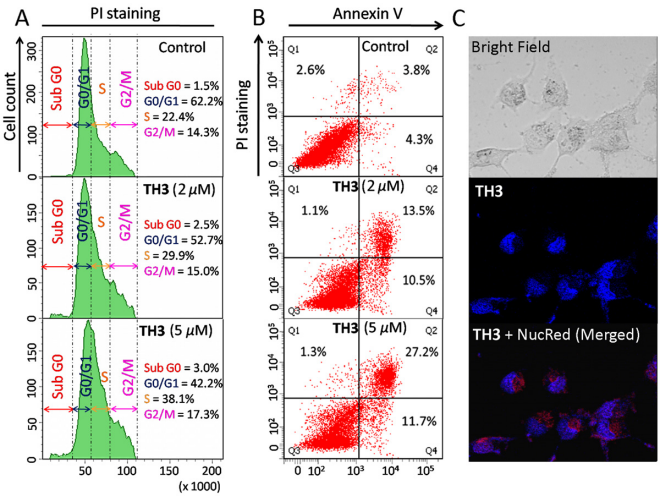

Figure 7. (**A**) Flow cytometric analysis of cell cycle parameters after incubation of HeLa cancer cells with **TH3** (2.0 and 5.0 μM). (**B**) Flow cytometric analysis of the mode of cancer cell death after treatment with **TH3** (2.0 and 5.0 μM) in HeLa cancer cells; Lower left (Q3), lower right (Q4), upper right (Q2) and upper left (Q1) quadrants indicate healthy cells, early, late apoptotic and necrotic cells, respectively. (**C**) Fluorescence microscopic image of localization of **TH3** (5.0 μM) in HeLa cell.

to control cells, treated with 0.1% DMSO), whereas **TH2** exhibited a small change in the *c-MYC* mRNA expression (0.72 fold, i.e. 28% decrease) relative to the control cells (treated with 0.1% DMSO). When 18S rRNA was used to normalize gene expression, similar results were obtained; the *c-MYC* mRNA levels were reduced to 0.7 fold and 0.3 fold by **TH2** and **TH3**, respectively. We have also monitored the *c-MYC* mRNA profiles upon treatment with peptides **TH2** and **TH3** in human alveolar basal epithelial cancer cells (A549) with respect to control GAPDH and 18S rRNA. The results show that **TH2** and **TH3** could reduce the *c-MYC* mRNA levels to ∼0.8- and ∼0.25-fold (i.e. decrease by 20% for **TH2** and decrease by 75% for **TH3**), respectively relative to the control cells (Supplementary Figure S24). In addition, the effect of peptides **TH2** and **TH3** was also studied on the expression of another G-quadruplex forming *BCL-2* oncogene. Interestingly, **TH2** and **TH3** did not induce any significant change in *BCL-2* mRNA (<25%) expression (Figure 6B). Furthermore, **TH2** and **TH3** did not essentially alter the mRNA levels of GAPDH and 18S rRNA. These results suggest that **TH3** inhibits the *c-MYC* transcription with three fold higher efficiency than **TH2** and further, both these peptides do not alter the expression of housekeeping genes.

Western blot. Western blot analysis was carried out to examine the effect of peptides **TH2** and **TH3** on the translation of *c-MYC* in HeLa cells (Figure 6C). Consistent with the qRT-PCR results, the densitometric analysis showed that **TH2** and **TH3**, at 5.0 μM concentration, reduced the *c-MYC* protein levels by ∼27% and ∼56%, respectively (Figure 6D), compared to the control cells. Importantly, the treatment of peptides **TH2** and **TH3** did not significantly alter the *BCL-2* gene expression at protein level (<25%) (Supplementary Figure S25). Furthermore, the protein levels of housekeeping GAPDH gene remained unchanged upon treatment with **TH2** and **TH3**. These results along with the qRT-PCR analysis indicate that the tripetide, **TH3** is more potent in reducing the *c-MYC* expression compared to the dipeptide **TH2**.

Dual-luciferase assay. In order to investigate the effect of these peptides (**TH2** and **TH3**) on the *c-MYC* gene expression, the dual-luciferase reporter assay was carried out (Figure 6E). The assay was performed using two reporter vectors containing (i) wild-type *c-MYC* G-quadruplex forming sequence in the upstream region of firefly luciferase coding gene (Del 4) and (ii) non G-quadruplex promoter sequence in the upstream region of renilla luciferase gene (pRL-TK). These two vectors were co-transfected into HeLa cells with subsequent treatment of 5 μM **TH2** or **TH3**. Owing to the absence of G-rich sequence in pRL-TK, the Renilla luciferase expression was unaffected by the peptides. The expression of *c-MYC* firefly luciferase was normalized relative to the Renilla luciferase expression. Our results suggest that peptide **TH3** decreased the wild-type (WT) *c-MYC* promoter-linked luciferase expression by 52%, relative to the untreated sample (Figure 6E). However, only a small change in the WT-*c-MYC* luciferase expression was observed upon treatment with **TH2** (Supplementary Figure S26).

To further validate our results, the effect of **TH2** and **TH3** on *c-MYC* firefly luciferase vector containing a mutated G-quadruplex promoter sequence (Mut-*c-MYC*) was also investigated (Supplementary Figure S26). Interestingly, we did not observe any notable change in Mut-*c-MYC* firefly luciferase expession upon treatment of **TH2** and **TH3** compared to the untreated control cells. In addition, **TH3** did not show any significant changes in the expression of reporter vector containing other promoter G-quadruplex forming sequences such as *BCL-2* (LB322 plasmid, Figure 6F). These results indicate that **TH3** downregulates *c-MYC* expression by directly targeting the *c-MYC* promoter quadruplex in cancer cells.

Antiproliferative activity of thiazole peptides in cancer cells

Cell cytotoxicity assay. As thiazole derivatives exhibit anticancer activities (49,50), we have evaluated the ability of thiazole peptides **TH2** and **TH3** to inhibit the growth of cancer cells. The growth inhibitory activities of peptides **TH2** and **TH3** for HeLa and A549 cancer cells as well as for normal human kidney epithelial cells (NKE) were investigated using XTT assay (Thermo scientific) (Supplementary Figures S27 and S28). Cells treated with 0.1% DMSO was used as control. **TH3** exhibited an IC_{50} value of 3.8 ± 0.6 μM for HeLa cells and 3.2 ± 0.4 μM for A549 cells, whereas **TH2** showed significantly higher IC_{50} values of 17.6 ± 2.8 μM and 15.8 ± 2.2 μM for HeLa and A549 cells, respectively. Comparatively, both ligands **TH2** and **TH3** exhibited negligible cytotoxicity for normal cells (IC50 ≥ 50 μM).

Cell cycle analysis. Flow cytometric analysis was conducted to examine whether the inhibitory effect of ligand **TH3** in HeLa cell proliferation was associated with cell cycle arrest (Figure 7A). The analysis of cell cycle histograms revealed an arrest in S phase population (22.4–38.1%) upon treatment with 5.0 μM **TH3**. The observed growth arrest in the S phase (Synthesis phase) by **TH3** indicates that it induces growth inhibition in HeLa cells.

Annexin V-FITC/PI apoptosis assay. The mode of cell death induced by peptide **TH3** was investigated by flow cytometry using Annexin V and PI dual staining assay (Figure 7B). HeLa cells were treated with various concentration of **TH3** (2.0 and 5.0 μM) for 24 h. The analyses of dot-plots show a dose dependent increase in the population of late apoptotic cells from ∼3.8% to ∼27.2% at 5.0 μM concentration of **TH3**. However, the population of necrotic cells decreases from ∼2.8% to ∼1.3% relative to the control cells (treated with 0.1% DMSO). These results indicate that G-quadruplex binding peptide **TH3** causes cancer cell death by inducing apoptosis.

Cell imaging using thiazole peptides. Fluorescence microscopy was employed to examine the cellular internalization and localization of **TH3** (Figure 7C). HeLa cells were treated with **TH3** (5.0 μM) for 2 h, and the fluorescence microscopic images were taken. The merged image shows that **TH3** localizes inside the nucleus. These results suggest that ligand **TH3** is cell membrane permeable and it binds to the cellular DNA.

CONCLUSION

In summary, we have synthesized novel thiazole peptides and demonstrated that a thiazole tripeptide, structurally related to distamycin A, selectively binds to *c-MYC* quadruplex over other investigated G-quadruplexes and duplex DNA. Intriguingly, NMR analysis suggests that two molecules of this crescent-shaped tripeptide bind to two terminals of *c-MYC* quadruplex; one molecule binds to the 5′-end and another one at the 3′-end. More importantly, the tripeptide significantly inhibits the transcription of the *c-MYC* oncogene by a quadruplex dependent mechanism. Since structurally related natural product distamycin derivatives are known as DNA binding ligands, the insights gained from this study would inspire the development of structural mimics of natural products for site-specific targeting of DNA structures.

SUPPLEMENTARY DATA

Supplementary Data are available at NAR Online.

ACKNOWLEDGEMENTS

We thank Department of Science and Technology (DST) and CSIR-India for funding. J.D. thanks DST for a SwarnaJayanti fellowship. D.D. thanks CSIR-India for research fellowship. M.D. and R.P. thank DST for INSPIRE fellowships. The authors thank DBT-IPLS unit, University of Calcutta for confocal microscopy. The work was supported by LOEWE program: SYNCHEMBIO and by iNEXT, project number 653706, funded by the Horizon 2020 program of the European Union. H.S. is member of the DFG-funded cluster of excellence: macromolecular complexes (EXC 115). Work at BMRZ is supported by the state of Hesse.
Author Contributions: All authors have given approval to the final version of the manuscript.

FUNDING

Department of Science and Technology [DST/SJF/CSA-01/2015-16]. Funding for open access charge: Institute of Organic Chemistry and Chemical Biology, Goethe University Frankfurt.
Conflict of interest statement. None declared.

REFERENCES

1. Collie,G.W. and Parkinson,G.N. (2011) The application of DNA and RNA G-quadruplexes to therapeutic medicines. *Chem. Soc. Rev.*, **40**, 5867–5892.
2. Bochman,M.L., Paeschke,K. and Zakian,V.A. (2012) DNA secondary structures: stability and function of G-quadruplex structures. *Nat. Rev. Genet.*, **13**, 770–780.
3. Hänsel-Hertsch,R., Di Antonio,M. and Balasubramanian,S. (2017) DNA G-quadruplexes in the human genome: detection, functions and therapeutic potential. *Nat. Rev. Mol. Cell Biol.*, **18**, 279–284.
4. Simonsson,T., Kubista,M. and Pecinka,P. (1998) DNA tetraplex formation in the control region of c-myc. *Nucleic Acids Res.*, **26**, 1167–1172.
5. Fernando,H., Reszka,A.P., Huppert,J., Ladame,S., Rankin,S., Venkitaraman,A.R., Neidle,S. and Balasubramanian,S. (2006) A conserved quadruplex motif located in a transcription activation site of the human c-kit oncogene. *Biochemistry*, **45**, 7854–7860.
6. Dexheimer,T.S., Sun,D. and Hurley,L.H. (2006) Deconvoluting the structural and drug-recognition complexity of the G-quadruplex-forming region upstream of the bcl-2 P1 promoter. *J. Am. Chem. Soc.*, **128**, 5404–5415.
7. Brooks,T.A. and Hurley,L.H. (2010) Targeting MYC expression through G-quadruplexes. *Genes Cancer*, **1**, 641–649.
8. Watson,J.D. and Crick,F.H.C. (1953) The structure of DNA. *Cold Spring Harbor Symp. Quantum Biol*, **18**, 123–131.
9. Phan,A.T., Modi,Y.S. and Patel,D.J. (2004) Propeller-type parallel-stranded G-quadruplexes in the human c-myc promoter. *J. Am. Chem. Soc.*, **126**, 8710–8716.
10. Ambrus,A., Chen,D., Dai,J., Jones,R.A. and Yang,D. (2005) Solution structure of the biologically relevant G-quadruplex element in the human *c-MYC* promoter. Implications for G-quadruplex stabilization. *Biochemistry*, **44**, 2048–2058.
11. Mathad,R.I., Hatzakis,E., Dai,J. and Yang,D. (2011) c-MYC promoter G-quadruplex formed at the 5′-end of NHE III 1 element: insights into biological relevance and parallel-stranded G-quadruplex stability. *Nucleic Acids Res.*, **39**, 9023–9033.
12. Siddiqui-Jain,A., Grand,C.L., Bearss,D.J. and Hurley,L.H. (2002) Direct evidence for a G-quadruplex in a promoter region and its targeting with a small molecule to repress c-MYC transcription. *Proc. Natl. Acad. Sci. U.S.A.*, **99**, 11593–11598.
13. Alzeer,J., Vummidi,B.R., Roth,P.J. and Luedtke,N.W. (2009) Guanidinium-Modified phthalocyanines as High-Affinity G-Quadruplex fluorescent probes and transcriptional regulators. *Angew. Chem. Int. Ed.*, **48**, 9362–9365.
14. Balasubramanian,S., Hurley,L.H. and Neidle,S. (2011) Targeting G-quadruplexes in gene promoters: a novel anticancer strategy? *Nat. Rev. Drug Discov.*, **10**, 261–275.
15. Agarwal,T., Roy,S., Chakraborty,T.K. and Maiti,S. (2010) Selective Targeting of G-Quadruplex Using Furan-Based Cyclic Homooligopeptides: Effect on c-MYC Expression. *Biochemistry*, **49**, 8388–8397.
16. Zeng,D.-Y., Kuang,G.-T., Wang,S.-K., Peng,W., Lin,S.-L., Zhang,Q., Su,X.-X., Hu,M.-H., Wang,H. and Tan,J.-H. (2017) Discovery of novel 11-Triazole substituted benzofuro [3, 2-b] quinolone derivatives as c-myc G-Quadruplex specific stabilizers via click chemistry. *J. Med. Chem.*, **60**, 5407–5423.
17. Debnath,M., Ghosh,S., Chauhan,A., Paul,R., Bhattacharyya,K. and Dash,J. (2017) Preferential targeting of i-motifs and G-quadruplexes by small molecules. *Chem. Sci.*, **8**, 7448–7456.
18. Kendrick,S., Muranyi,A., Gokhale,V., Hurley,L.H. and Rimsza,L.M. (2017) Simultaneous drug targeting of the promoter MYC G-Quadruplex and BCL2 i-Motif in diffuse large B-Cell lymphoma delays tumor growth. *J. Med. Chem.*, **60**, 6587–6597.
19. Wang,M., Mao,Z., Kang,T.-S., Wong,C.-Y., Mergny,J.-L., Leung,C.-H. and Ma,D.-L. (2016) Conjugating a groove-binding motif to an Ir (III) complex for the enhancement of G-quadruplex probe behavior. *Chem. Sci.*, **7**, 2516–2523.
20. Nanjunda,R., Musetti,C., Kumar,A., Ismail,M.A., Farahat,A.A., Wang,S., Sissi,C., Palumbo,M., Boykin,D.W. and Wilson,W.D. (2012) Heterocyclic dications as a new class of telomeric G-Quadruplex targeting agents. *Curr. Pharm. Des.*, **18**, 1934–1947.
21. Ma,D.-L., Chan,D.S.-H., Fu,W.-C., He,H.-Z., Yang,H., Yan,S.-C. and Leung,C.-H. (2012) Discovery of a natural Product-Like c-myc G-Quadruplex DNA Groove-Binder by molecular docking. *PLOS ONE*, **7**, e43278.
22. Huang,J., Li,G., Wu,Z., Song,Z., Zhou,Y., Shuai,L., Weng,X., Zhou,X. and Yang,G. (2009) Bisbenzimidazole to benzobisimidazole: from binding B-form duplex DNA to recognizing different modes of telomere G-quadruplex. *Chem. Commun.*, 902–904.
23. Jain,A.K. and Bhattacharya,S. (2011) Interaction of G-Quadruplexes with nonintercalating Duplex-DNA minor groove binding ligands. *Bioconjugate Chem.*, **22**, 2355–2368.
24. De Cian,A., Guittat,L., Kaiser,M., Saccà,B., Amrane,S., Bourdoncle,A., Alberti,P., Teulade-Fichou,M.-P., Lacroix,L. and Mergny,J.-L. (2007) Fluorescence-based melting assays for studying quadruplex ligands. *Methods*, **42**, 183–195.
25. Liu,M., Mao,X.-A., Ye,C., Huang,H., Nicholson,J.K. and Lindon,J.C. (1998) Improved WATERGATE pulse sequences for solvent suppression in NMR spectroscopy. *J. Magn. Reson.*, **132**, 125–129.

26. Sklenář,V. and Bax,A. (1987) Spin-echo water suppression for the generation of pure-phase two-dimensional NMR spectra. *J. Magn. Reson.*, **74**, 469–479.
27. Palmer,A.G. III, Cavanagh,J., Wright,P.E. and Rance,M. (1990) Sensitivity improvement in Proton-Detected Two-Dimensional heteronuclear correlation NMR spectroscopy heteronuclear correlation NMR spectroscopy. *J. Magn. Reson.*, **93**, 151–170.
28. Kay,L., Keifer,P. and Saarinen,T. (1992) Pure absorption gradient enhanced heteronuclear single quantum correlation spectroscopy with improved sensitivity. *J. Am. Chem. Soc.*, **114**, 10663–10665.
29. Hwang,T.L. and Shaka,A.J. (1995) Water suppression that works. Excitation sculpting using arbitrary Wave-Forms and Pulsed-Field gradients. *J. Magn. Reson.*, **112**, 275–279.
30. Lowry,O.H., Rosebrough,N.J., Farr,A.L. and Randall,R.J. (1951) Protein measurement with the folin phenol reagent. *J. Biol. Chem.*, **193**, 265–275.
31. Roy,R.S., Gehring,A.M., Milne,J.C., Belshaw,P.J. and Walsh,C.T. (1999) Thiazole and oxazole peptides: biosynthesis and molecular machinery. *Nat. Prod. Rep.*, **16**, 249–263.
32. Hamada,Y. and Shioiri,T. (2005) Recent progress of the synthetic studies of biologically active marine cyclic peptides and depsipeptides. *Chem. Rev.*, **105**, 4441–4482.
33. Bagley,M.C., Dale,J.W., Merritt,E.A. and Xiong,X. (2005) Thiopeptide antibiotics. *Chem. Rev.*, **105**, 685–714.
34. Brockmann,A., Strittmatter,T., May,S., Stemmer,K., Marx,A. and Brunner,T. (2014) Structure–Function relationship of Thiazolide-Induced apoptosis in colorectal tumor cells. *ACS Chem. Biol.*, **9**, 1520–1527.
35. Padroni,G., Parkinson,J.A., Fox,K.R. and Burley,G.A. (2018) Structural basis of DNA duplex distortion induced by thiazole-containing hairpin polyamides. *Nucleic Acids Res.*, **46**, 42–53.
36. García-Reynaga,P. and VanNieuwenhze,M.S. (2008) A new total synthesis of patellamide A. *Org. Lett.*, **10**, 4621–4623.
37. Banker,R. and Carmeli,S. (1998) Tenuecyclamides A– D, cyclic hexapeptides from the cyanobacterium nostoc spongiaeforme var. tenue. *J. Nat. Prod.*, **61**, 1248–1251.
38. Todorova,A.K., Juettner,F., Linden,A., Pluess,T. and von Philipsborn,W. (1995) Nostocyclamide: a new macrocyclic, thiazole-containing allelochemical from Nostoc sp. 31 (cyanobacteria). *J. Org. Chem.*, **60**, 7891–7895.
39. Tera,M., Ishizuka,H., Takagi,M., Suganuma,M., Shin-ya,K. and Nagasawa,K. (2008) Macrocyclic hexaoxazoles as Sequence-and Mode-Selective G-Quadruplex binders. *Angew. Chem. Int. Ed.*, **47**, 5557–5560.
40. Meunier,B. (2007) Hybrid molecules with a dual mode of action: dream or reality? *Acc. Chem. Res.*, **41**, 69–77.
41. Kim,M.-Y., Vankayalapati,H., Shin-Ya,K., Wierzba,K. and Hurley,L.H. (2002) Telomestatin, a potent telomerase inhibitor that interacts quite specifically with the human telomeric intramolecular G-quadruplex. *J. Am. Chem. Soc.*, **124**, 2098–2099.
42. Jantos,K., Rodriguez,R., Ladame,S., Shirude,P.S. and Balasubramanian,S. (2006) Oxazole-based peptide macrocycles: a new class of G-quadruplex binding ligands. *J. Am. Chem. Soc.*, **128**, 13662–13663.
43. Rzuczek,S.G., Pilch,D.S., Liu,A., Liu,L., LaVoie,E.J. and Rice,J.E. (2010) Macrocyclic pyridyl polyoxazoles: selective RNA and DNA G-quadruplex ligands as antitumor agents. *J. Med. Chem.*, **53**, 3632–3644.
44. Cocco,M.J., Hanakahi,L.A., Huber,M.D. and Maizels,N. (2003) Specific interactions of distamycin with G-quadruplex DNA. *Nucleic Acids Res.*, **31**, 2944–2951.
45. Hatzakis,E., Okamoto,K. and Yang,D. (2010) Thermodynamic stability and folding kinetics of the major G-quadruplex and its loop isomers formed in the nuclease hypersensitive element in the human c-Myc promoter: effect of loops and flanking segments on the stability of parallel-stranded intramolecular G-quadruplexes. *Biochemistry*, **49**, 9152–9160.
46. Kumar,Y.P., Bhowmik,S., Das,R.N., Bessi,I., Paladhi,S., Ghosh,R., Schwalbe,H. and Dash,J. (2013) A fluorescent guanosine dinucleoside as a selective Switch-On sensor for c-myc G-Quadruplex DNA with potent anticancer activities. *Chem. Eur. J.*, **19**, 11502–11506.
47. Cosconati,S., Marinelli,L., Trotta,R., Virno,A., De Tito,S., Romagnoli,R., Pagano,B., Limongelli,V., Giancola,C., Baraldi,P.G. *et al.* (2010) Structural and conformational requisites in DNA quadruplex groove binding: another piece to the puzzle. *J. Am. Chem. Soc.*, **132**, 6425–6433.
48. Martino,L., Virno,A., Pagano,B., Virgilio,A., Di Micco,S., Galeone,A., Giancola,C., Bifulco,G., Mayol,L. and Randazzo,A. (2007) Structural and thermodynamic studies of the interaction of distamycin A with the parallel quadruplex structure $[d(TGGGGT)]_4$. *J. Am. Chem. Soc.*, **129**, 16048–16056.
49. Lombardo,L.J., Lee,F.Y., Chen,P., Norris,D., Barrish,J.C., Behnia,K., Castaneda,S., Cornelius,L.A., Das,J. and Doweyko,A.M. (2004) Discovery of N-(2-chloro-6-methyl-phenyl)-2-(6-(4-(2-hydroxyethyl)-piperazin-1-yl)-2-methylpyrimidin-4-ylamino) thiazole-5-carboxamide (BMS-354825), a dual Src/Abl kinase inhibitor with potent antitumor activity in preclinical assays. *J. Med. Chem.*, **47**, 6658–6661.
50. Lu,Y., Li,C.-M., Wang,Z., Chen,J., Mohler,M.L., Li,W., Dalton,J.T. and Miller,D.D. (2011) Design, synthesis, and SAR studies of 4-substituted methoxylbenzoyl-aryl-thiazoles analogues as potent and orally bioavailable anticancer agents. *J. Med. Chem.*, **54**, 4678–4693.